Fermi hypernetted-chain theory for correlated spin-density-wave states

X. Q. G. Wang
International School for Advanced Studies, 34014 Trieste, Italy

S. Fantoni
International School for Advanced Studies, 34014 Trieste, Italy
and Istituto Nazionale di Fisica Nucleare, Sezione di Trieste, Trieste, Italy

E. Tosatti
International School for Advanced Studies, 34014 Trieste, Italy
and International Centre for Theoretical Physics, 34100 Trieste, Italy

L. Yu
International Centre for Theoretical Physics, 34100 Trieste, Italy
and Institute of Theoretical Physics, Academia Sinica, 100080 Beijing, China
(Received 27 April 1992)

The Fermi hypernetted-chain (FHNC) theory is applied to spin-density-wave states combined with a Jastrow-type correlation operator. The commonly used approximation scheme FHNC/n is found to be unsuitable for dealing with this class of correlated wave functions. A new scheme, named FHNC-n, is proposed, and numerically tested for the one-dimensional (1D) Hubbard model and the Gutzwiller correlation operator. The results obtained are in very good agreement with the available variational Monte Carlo calculation. This scheme can be used to study 2D and 3D Hubbard models and can easily be extended to treat more general correlation operators, which include triplet and quartet correlations.

I. INTRODUCTION

In the past decades, the quantitative understanding of the correlation effects in strongly interacting systems has been one of the main issues in many-body physics. Particularly, much effort has been devoted to electron systems in connection with phenomena such as heavy-fermion dynamics, quantum Hall effects, metal-insulator transition, and high-T_c superconductivity. It has been shown that strong correlation effects can hardly be handled by means of conventional perturbation theories, namely, those built upon independent particle basis functions.

Green-function Monte Carlo (GFMC) theory[1] or other stochastic methods,[2,3] as well as perturbative approaches based on correlated basis function (CBF) theory,[4–6] have been highly developed in the last few years and one may hope that they will provide, in the near future, accurate numerical solutions for some strongly interacting Fermi systems.

The variational approach, even though less fundamentally based, is also very powerful, since it is applicable to both Bose and Fermi systems, irrespective of the strength of the interaction. It allows modeling the trial wave function according to the main physical features expected for the system under consideration. Therefore, it is very useful in understanding the role played by a certain type of correlations, like, for instance, two-body (Jastrow), many-body, spin-spin, etc. Moreover, realistic variational wave functions provide very convenient starting points for further GFMC and CBF studies.

The variational ground state for an interacting Fermi system is usually taken of the form

$$|\Psi_0\rangle=\hat{F}|\Phi_m\rangle\ , \tag{1.1}$$

where $|\Phi_m\rangle$ is a reference state which can be expressed as a Slater determinant of single-particle states determined by a mean-field (MF) approximation. $\hat{F}$ is a correlation operator projecting onto $|\Phi_m\rangle$ the correlations which are absent in $|\Phi_m\rangle$, and which are thought to be physically relevant. Many types of reference states, besides the ordinary paramagnetic state $|\Phi_P\rangle$, are expected to be useful, in view of the rich physics of a strongly interacting system, whose simplest prototype is the Hubbard model. Among them $|\Phi_m\rangle$ can be a BCS state, a commensurate spin-density wave $|\Phi_{\rm SDW}\rangle$,[7] a spiral spin-density wave,[8] etc.

A correlation operator of the Jastrow form,

$$\hat{F}_J=\prod_{i<j} f(\mathbf{r}_{ij})\ , \tag{1.2}$$

embodies the main two-body dynamical correlations, although many-body and state-dependent correlations have been found to be important as well, especially in dense systems. In the case of on-site correlations in a lattice system, $\hat{F}_J$ reduces to the Gutzwiller projection operator:

$$f(i,j)=1-(1-g)\delta_{r_{i\uparrow},r_{j\downarrow}}\ . \tag{1.3}$$

In variational calculations, either Monte Carlo technique or the Fermi hypernetted chain (FHNC) theory can be used to evaluate the energy expectation value. In fact,

both of them have been used for several strongly interacting continuous systems, like liquid helium or nuclear matter,[4] as well as in the case of lattice electron systems.[9–11]

The interest of a FHNC-type of calculation is related (i) to the possibility of avoiding a finite-size problem by working directly in the thermodynamic limit, (ii) to the possibility of finding the optimal pair correlation function for a given reference state and, most of all, (iii) to developing the necessary starting point and the techniques for future CBF calculations, where the nondiagonal matrix elements of the Hamiltonian are also required.

Particularly, one would like to verify the feasibility of FHNC theory in the test case of the Hubbard Hamiltonian,[12,13] which is well known to describe intrinsic properties such as the itinerant magnetism and metal-insulator transition[14] and is also regarded as a fundamental model related to the electronic and magnetic properties of high-T_c oxide superconductors.[13] Recently, the FHNC scheme has been implemented for the Hubbard discrete lattice model.[11] The results for the one-dimensional (1D) Gutzwiller correlated Fermi sea wave function are in good agreement with the corresponding variational Monte Carlo estimates[10] for intermediate values of the strength U/t. However, this starting point has many shortcomings, including lack of insulating behavior, and the presence of a related Fermi jump in the momentum distribution, even at half-filling.

In this paper, we apply FHNC theory to correlated spin-density-wave function $\hat{F}|\Phi_{\rm SDW}\rangle$. The commensurate SDW state is a band insulator at half-filling, and has an antiferromagnetic long-range order (ALFRO), which persists in the correlated state $\Psi_{\rm SDW}$. The SDW state has been recently reconsidered by Schrieffer *et al.*[7] in connection with the spin-bag model of high-T_c superconductivity. $|\Phi_{\rm SDW}\rangle$ is a Slater determinant of single-particle wave functions.[10]

$$\psi_{\mathbf{k}\sigma}(r_i)=[u(\mathbf{k})e^{i\mathbf{k}\cdot\mathbf{r}_i}+\hat{\sigma}_z(i)v(\mathbf{k})e^{i(\mathbf{k}+\mathbf{Q})\cdot\mathbf{r}_i}]\xi_\sigma(i)\ , \tag{1.4}$$

for $\mathbf{k}$ embedded in the Fermi sea (FS), where $\mathbf{Q}$ is the antiferromagnetic nesting vector. For a single two-sublattice antiferromagnetic structure, $\mathbf{Q}$ is defined by the condition $e^{i\mathbf{Q}\cdot\mathbf{r}_i}=-1$ for all translations τ which transform one sublattice into the other. Thus, $\mathbf{Q}$ is π/a for 1D. The coefficients $u(k)$ and $v(k)$ are variational functions subject to the orthonormalization condition $u^2(k)+v^2(k)=1$. A convenient parametrization of $u(k)$ and $v(k)$ is provided by the mean-field solutions:

$$u(k)=\left[\frac{1}{2}\left[1+\frac{\epsilon(k)}{E_0(k)}\right]\right]^{1/2},\qquad v(k)=\left[\frac{1}{2}\left[1-\frac{\epsilon(k)}{E_0(k)}\right]\right]^{1/2}, \tag{1.5}$$

where $E_0(k)=[\epsilon^2(k)+\Delta^2]^{1/2}$ is the energy of quasiparticle and $\epsilon(k)=-2t\cos k_x a$ for 1D. In this parametrization, the gap Δ is the only variational parameter in the reference state. Obviously, if $\Delta=0$, $\Phi_{\rm SDW}$ coincides with the paramagnetic state.

In spite of the fact that, as is well known, the Gutzwiller correlation operator is not able to describe all the ground-state properties of the 1D Hubbard model,[15–17] much effort has been devoted to variational calculation with this trial wave function, since it provides a reasonable estimate for the energy upper bound in the 1D and 2D Hubbard models.

Most notably, for the 1D Gutzwiller correlation operator and $|\Phi_P\rangle$ (i.e., $\Delta=0$), Metzner and Vollhardt[18] have provided exact analytic expressions for the expectation value of the Hubbard Hamiltonian as a function of g. Moreover, very detailed variational Monte Carlo (VMC) calculations[10] have been performed by Yokoyama and Shiba for several values of Δ.

In this paper, we discuss a FHNC scheme which can be used for the full Jastrow operator and easily extended to the case of a more complex correlation operator. We limit our numerical analysis to the 1D case and the Gutzwiller operator, for the sake of comparison with existing calculations.[10,18]

The standard FHNC theory, derived in the present paper for the correlated SDW function, cannot be expressed in a closed form similar to the other existing FHNC summations because of the structure of the elementary diagrams E. A commonly used approximation scheme is the so-called FHNC/n,[4] where n denotes the highest rank of elementary diagrams included in the calculation. For instance, E is completely neglected in FHNC/0. Only four-body elementary diagrams are included in FHNC/4 and so on.

It turns out that FHNC/n is a slowly converging sequence. At $\Delta=0$, FHNC/0 does provide results which are in reasonable agreement with the available Monte Carlo estimate for $U/t\leq 8$.[11] However, for larger U/t, FHNC/0 is not satisfactory, and FHNC/4 improves the agreement only very little. For $\Delta>0$ and growing, FHNC/0 begins to fail at lower and lower values of U/t.

We propose in this paper a variant of the FHNC scheme, denoted as FHNC-n, which differs from the usual FHNC/n scheme in that all of the elementary diagrams included at a given order are characterized by the number of dynamical correlations $h(\mathbf{r}_{ij})=f^2(\mathbf{r}_{ij})-1$, rather than by the number of particle variables. For instance, the FHNC-2 approximation includes all the elementary diagrams with, at most, two h factors, and they may involve up to six particle variables. Such a scheme is inspired by the power series[19] (PS) cluster expansion, in which the nth order includes all irreducible cluster terms with a number $m\leq n$ of $h(\mathbf{r}_{ij})$ factors. In fact, at each order of the PS expansion the uncorrelated distribution functions entering into the cluster terms are treated exactly, and, as a consequence, important sum rules (like, for instance, the sequential and the normalization sum rules) are exactly fulfilled. The need of such a scheme has also been envisaged in a calculation on continuous systems, for instance, 3D electron gas,[20] liquid ^{3}He,[21] and finite nuclei.[22] This requirement is particularly stringent in lattice systems,[23] particularly in the case of the SDW reference state characterized by strong statistical correlations. For instance, for any nonzero value of Δ, both FHNC/0 and FHNC/4 badly violate the sum rules,

whereas they are almost exactly satisfied in each FHNC-n approximation. However, while satisfying the sum rules at each order, the PS expansion is unfortunately again very slowly converging in the strong-coupling regime. The convergence of FHNC-n seems to be better. Therefore, the FHNC-n approach suggests itself as the only viable way to handle the SDW-type wave functions.

The rest of this paper is arranged as follows. The formal FHNC theory for correlated SDW functions is presented in Sec. II. The FHNC-n scheme is discussed in Sec. III. The calculation for the 1D Hubbard model for a Gutzwiller correlated SDW function is discussed in Sec. IV. It is shown there that, for example, FHNC-3 provides results which agree with the analytic and the VMC results within few percent, and that the FHNC-2 approximation can safely be used during the minimization process. Moreover, it is shown that the sum rules are very well satisfied. Section V is left to the discussion and the conclusions.

II. THE FHNC THEORY FOR THE HUBBARD MODEL WITH CORRELATED SPIN-DENSITY WAVE

The Hubbard model is defined by the lattice Hamiltonian[12,13]

$$H=-t\sum_{\langle i,j\rangle,\sigma}c_{i\sigma}^{\dagger}c_{j\sigma}+U\sum_{i}n_{i\uparrow}n_{i\downarrow}\ , \tag{2.1}$$

where $c_{i\sigma}^{\dagger}$ ($c_{i\sigma}$) is the creation (annihilation) operator of an electron with spin $\sigma=\pm\frac{1}{2}$ on site i; t and U represent the nearest-neighbor hopping energy and the on-site Coulomb repulsive interaction with opposite spin, respectively. The variational ground-state energy can be expressed in the form[11]

$$E_0=\langle T\rangle+\langle V\rangle\ , \tag{2.2}$$

$$\langle T\rangle/N=-zt\rho n(\mathbf{a})=-zt\rho\sum_{k}\epsilon(\mathbf{k})n(\mathbf{k})\ , \tag{2.3}$$

$$\langle V\rangle/N=U\rho^2g(0)/2\ , \tag{2.4}$$

where $\mathbf{a}=\sum_i^D I_i\hat{\mathbf{e}}_i$ is the unit vector for the lattice, z is the coordination number in the D-dimensional lattice system, and $\rho=A/N$ is actually twice the filling factor. The functions $g(r_{ij})$ and $n(r_{ij})$ are the pair distribution function and the one-body density matrix, respectively. These two quantities are also directly used to express the two-body static structure function $S(\mathbf{k})=\langle\rho_{\mathbf{k}}^{\dagger}\rho_{\mathbf{k}}\rangle$, with $\rho_{\mathbf{k}}=(1/\sqrt{A})\sum_i\exp(i\mathbf{k}\cdot\mathbf{r}_i)$, given by

$$S(\mathbf{k})=1+\rho\sum_{\mathbf{r}}[g(\mathbf{r})-1]\cos(\mathbf{k}\cdot\mathbf{r})\ , \tag{2.5}$$

and the momentum distribution function $n(\mathbf{q})$

$$n(\mathbf{q})=\frac{1}{\nu}\sum_{r}n(\mathbf{r})\cos(i\mathbf{q}\cdot\mathbf{r})\ . \tag{2.6}$$

The following sum rules must be obeyed by $S(\mathbf{k})$ and $n(\mathbf{k})$:

$$S(0)=0\ , \tag{2.7}$$

$$\sum_{\mathbf{k}\in\mathrm{BZ}}\nu n(r=0)=1\ . \tag{2.8}$$

We present in the following two subsections the FHNC theories for the pair distribution function $g(\mathbf{r}_{12})$ and the one-body distribution $n(\mathbf{r}_{11'})$ for the correlated SDW state.

A. FHNC scheme for $g(\mathbf{r}_{ij})$

The cluster expansion of the pair distribution function is obtained by first expressing[24,4] F_J^2 as a sum of cluster terms:[19]

$$F_J^2=\prod_{i<j}f^2(\mathbf{r}_{ij})$$
$$=X_2(\mathbf{r}_1,\mathbf{r}_2)+\sum_{i>2}X_3(\mathbf{r}_1,\mathbf{r}_2,\mathbf{r}_i)+\cdots\ , \tag{2.9}$$

where

$$X_2(\mathbf{r}_1,\mathbf{r}_2)=f^2(r_{12})\ , \tag{2.10}$$

$$X_3(\mathbf{r}_1,\mathbf{r}_2,\mathbf{r}_i)=f^2(r_{12})[h(\mathbf{r}_{1i})+h(\mathbf{r}_{2i})+h(\mathbf{r}_{1i})h(\mathbf{r}_{2i})]\ . \tag{2.11}$$

Similar expressions are found for $X_{p>3}$ clusters. It turns out that $g(\mathbf{r}_{12})$ is given by

$$g(\mathbf{r}_{12})=\frac{1}{\mathcal{N}}\rho^2\sum_{p}\frac{\rho^p}{(p-2)!}\sum_{\mathbf{r}_3,\ldots,\mathbf{r}_p}X_p(\mathbf{r}_1,\ldots,\mathbf{r}_p)\times\mathcal{D}_p(\mathbf{r}-1,\ldots,\mathbf{r}_p)\ , \tag{2.12}$$

where $\mathcal{D}_p$ are the p-body uncorrelated distribution functions:

$$\mathcal{D}_p(\mathbf{r}_1,\ldots,\mathbf{r}_p)=\frac{A(A-1)(A-p+1)}{\rho^p}\frac{\sum_{\mathbf{r}_{p+1}\cdots\mathbf{r}_N}|\Phi_{\mathrm{SDW}}|^2}{\sum_{\mathbf{r}_1\cdots\mathbf{r}_N}|\Phi_{\mathrm{SDW}}|^2}\ , \tag{2.13}$$

and $\mathcal{N}=\langle\Psi_{\mathrm{SDW}}|\Psi_{\mathrm{SDW}}\rangle$ is a normalization factor. The Hartree-Fock results is obtained by setting $X_2=1$ and $X_{p>3}=0$. As in the ordinary paramagnetic case, $\mathcal{D}_P$ can be expressed in terms of the uncorrelated density matrix:

$$\hat{\rho}(1,2)=\frac{1}{N}\sum_{\mathbf{k}\in\mathrm{FS},\sigma}\phi_{\mathbf{k}\sigma}^{\dagger}(1)\phi_{\mathbf{k}\sigma}(2)$$
$$=\sum_{\sigma}\xi_{\sigma}^{\dagger}(1)\xi_{\sigma}(2)[l_u(\mathbf{r}_{12})+e^{i\mathbf{Q}\cdot\mathbf{r}_1}l_v(\mathbf{r}_{12})\mathrm{sgn}(\sigma)]\ , \tag{2.14}$$

where $\mathrm{sgn}(\sigma)$ takes either $+1$ or -1 corresponding to spin state $\xi_\sigma=\uparrow$ or $\downarrow$, and

$$l_u(\mathbf{r}_{12})=\frac{1}{N}\sum_{\mathbf{k}\in\mathrm{FS}}e^{-i\mathbf{k}\cdot\mathbf{r}_{12}}\{u^2(\mathbf{k})+v^2(\mathbf{k})\cos(\mathbf{Q}\cdot\mathbf{r}_{12})\}\ , \tag{2.15}$$

$$l_v(\mathbf{r}_{12})=\frac{1}{N}\sum_{\mathbf{k}\in\mathrm{FS}}u(\mathbf{k})v(\mathbf{k})e^{-i\mathbf{k}\cdot\mathbf{r}_{12}}[1+\cos(\mathbf{Q}\cdot\mathbf{r}_{12})]\ . \tag{2.16}$$

The density matrices $\hat{\rho}(i,j)$ appear in $\mathcal{D}_p$ in the form of closed separate loops, each with a factor $-(-1/\rho)^m$, m being the number of loop points. The loops with $m>2$ have an extra factor 2, since they originate from two different cyclic permutations. Since the dynamical correlations are spin independent they do not affect the spin traces and one has

$$\mathcal{D}_P=1-\left[\frac{1}{\rho}\right]^2\sum_{i<j}\hat{\rho}(i,j)\hat{\rho}(j,i)+2\left[\frac{1}{\rho}\right]^3\sum_{i<j<k}\hat{\rho}(i,k)\hat{\rho}(k,j)\hat{\rho}(j,i)+\cdots . \tag{2.17}$$

It follows that $\rho^2\mathcal{N}g(r_{12})$ is given by a series of cluster terms, each being a product of dynamical correlations and exchange operators, so that each particle variable of the cluster, except for $\mathbf{r}_1$ and $\mathbf{r}_2$, is an argument of at least one dynamical correlation. For every p value, in Eq. (2.12) there are $(p-2)!/S$ cluster terms, which differ only in the way of labeling the $p-2$ indices (S is the symmetry number, namely, the number of permutations of the internal points, which leave the corresponding cluster term unchanged). One can then remove the $(p-2)!$ factor in Eq. (2.12) and sum over the topologically distinct cluster terms.

The linked cluster theorem ensures that $\rho^2\mathcal{N}g(\mathbf{r}_{12})$ is a sum of linked cluster terms $f^2(\mathbf{r}_{12})$ times $\mathcal{N}$. The separability theorem, based on the property $\sum_{\mathbf{r}_k\sigma_k}\hat{\rho}(i,k)\hat{\rho}(k,j)=\hat{\rho}(i,j)$, implies that all the separable cluster terms of $g(\mathbf{r}_{12})$ cancel each other, with the result

$$g(\mathbf{r}_{12})=\frac{1}{\rho^2}f^2(\mathbf{r}_{12})\sum_p\rho^p\sum_{\mathbf{r}_3,\ldots,\mathbf{r}_p}\mathcal{J}_g^{(p)}(\mathbf{r}_1,\ldots,\mathbf{r}_p) . \tag{2.18}$$

A few examples of cluster diagrams representing $\mathcal{J}_g^{(p)}$ are shown in Fig. 1.

The FHNC scheme for calculating $g(\mathbf{r}_{12})$ is very similar to that developed for the ordinary paramagnetic case.[11] The chain equations for N_{dd}, N_{de}, and N_{ee} are exactly the same as in Ref. 11 and therefore will not be repeated here. On the other hand, because of the two-component structure of $\hat{\rho}(i,j)$ and because of the presence of the phase factor $e^{i\mathbf{Q}\cdot\mathbf{r}_i}$, the calculation of the (cyclic-cyclic) chain diagrams $\hat{N}_{cc}$ and of the composite diagrams $\hat{X}_{cc}$ and X_{ee} requires some more discussion. It is useful to represent the cyclic diagrams with two-component vector quantities of the form

$$\hat{Z}(i,j)\equiv[Z_u(\mathbf{r}_{ij}),Z_v(\mathbf{r}_{ij})]=\sum_\sigma\xi_\sigma^\dagger(i)\xi_\sigma(j)\{Z_u(\mathbf{r}_{ij})+\mathrm{sgn}(\sigma)e^{i\mathbf{Q}\cdot\mathbf{r}_i}Z_v(\mathbf{r}_{ij})\} . \tag{2.19}$$

The components of $\hat{\rho}(i,j)$ are given by $l_u(\mathbf{r}_{ij})$ and $l_v(\mathbf{r}_{ij})$, respectively. The convolution integral is defined as

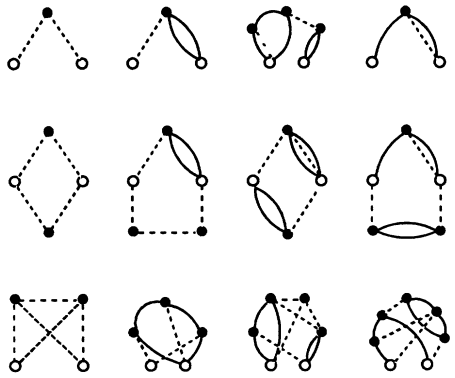

FIG. 1. Examples of cluster diagrams contributing to $g(\mathbf{r}_{12})$. The open dots represent the external variables 1 and 2, whereas the solid dots denote internal variables, upon which summation is implied. Dashed and oriented solid lines represent the dynamical correlation $h(r_{ij})$ and exchange operator $\hat{\rho}(i,j)$, respectively. The diagrams in the first row are chain (nodal), those in the second row are composite and the diagrams in the bottom row are elementary diagram which are of four, five, six, and seven body, respectively. Diagrams in the first column are of the *dd* type; the *de*, *ee*, and *cc* diagrams are displayed in the subsequent columns.

$$\hat{Z}(i,j)=[\hat{F}(i,k)|\hat{G}|(k,j)] , \tag{2.20}$$

$$Z_u(\mathbf{r}_{ij})=\rho\sum_{\mathbf{r}_k}\{F_u(r_{ik})G_u(r_{kj})+F_v(r_{ik})G_v(r_{kj})\cos(\mathbf{Q}\cdot\mathbf{r}_{ik})\} , \tag{2.21}$$

$$Z_v(\mathbf{r}_{ij})=\rho\sum_{\mathbf{r}_k}\{F_v(r_{ik})G_u(r_{kj})+F_u(r_{ik})G_v(r_{kj})\cos(\mathbf{Q}\cdot\mathbf{r}_{ik})\} , \tag{2.22}$$

while the closed-loop parallel connection between two vector quantities is a scalar given by

$$\hat{F}(i,j)*\hat{G}(i,j)=2F_u(r_{ij})G_u(r_{ij})+2\cos(\mathbf{Q}\cdot\mathbf{r}_{ij})F_v(r_{ij})G_v(r_{ij}) . \tag{2.23}$$

In doing the chain summation one has to keep track of the ordering of the various *cc* elements due to the asymmetrical structure of convolution integral [Eqs. (2.19)–(2.22)], with the result

$$\hat{N}_{cc}(i,j)=\{\hat{N}_{\rho a}(i,k)|\hat{X}_{cc}(k,j)-[\hat{X}_{cc}(k,l)|(1/\nu)\hat{\rho}(l,j)]\}+[\hat{X}_{cc}(i,k)|\hat{N}_{a\rho}(k,j)]+[\hat{N}_{ca}(i,k)|\hat{X}_{cc}(k,j)] , \tag{2.24}$$

where the chain operators $\hat{N}_{\rho a}$ and $\hat{N}_{ca}$ have $-1/\nu\hat{\rho}$ and $\hat{X}_{cc}$ as their first chain elements (having i as a particle variable), respectively. $\hat{N}_{\rho a}$ and $\hat{N}_{ca}$ are given by

$$\hat{N}_{\rho a}(i,j)=-(1/\nu)\hat{\rho}(i,j)+\{\hat{N}_{\rho a}(i,k)|\hat{X}_{cc}(k,j)-[\hat{X}_{cc}(k,l)|(1/\nu)\hat{\rho}(l,j)]\}\ , \tag{2.25}$$

$$\hat{N}_{ca}(i,k)=\hat{X}_{cc}(i,j)-[\hat{X}_{cc}(i,k)|(1/\nu)\hat{\rho}(k,j)]+\{\hat{N}_{ca}(i,k)|\hat{X}_{cc}(k,j)-[\hat{X}_{cc}(k,l)|(1/\nu)\hat{\rho}(l,j)]\}\ . \tag{2.26}$$

The equation for $\hat{N}_{cc}$ reduces to the conventional FHNC equation for $N_{cc}(r_{ij})$ when $l_v(r_{ij})=0$. The composite diagrams $\hat{X}_{cc}$ and X_{ee} are summed by

$$\hat{X}_{cc}(i,j)=[g_{dd}(\mathbf{r}_{ij})-1][\hat{N}_{cc}(i,j)-(1/\nu)\hat{\rho}(i,j)]+g_{dd}(\mathbf{r}_{ij})\hat{E}_{cc}(i,j)\ , \tag{2.27}$$

$$X_{ee}(\mathbf{r}_{ij})=g_{dd}(\mathbf{r}_{ij})\{N_{ee}(\mathbf{r}_{ij})+E_{ee}(\mathbf{r}_{ij})+[N_{de}(\mathbf{r}_{ij})+E_{de}(\mathbf{r}_{ij})]^2 -2[\hat{N}_{cc}(i,j)+\hat{E}_{cc}(i,j)-(1/\nu)\hat{\rho}(i,j)]^2\}-N_{ee}(\mathbf{r}_{ij})\ , \tag{2.28}$$

where $g_{dd}(\mathbf{r}_{ij})=f^2(r_{ij})\exp\{N_{dd}(\mathbf{r}_{ij})+E_{dd}(\mathbf{r}_{ij})\}$, and $E_{\alpha\beta}(i,j)$ refers to the sum of elementary diagrams of $\alpha\beta$ type.

In terms of the FHNC quantities, the pair distribution function is given by

$$g(\mathbf{r}_{12})=1+X_{dd}(\mathbf{r}_{12})+N_{dd}(\mathbf{r}_{12})+2X_{de}(\mathbf{r}_{12})+2N_{de}(\mathbf{r}_{12}) +N_{ee}(\mathbf{r}_{12})+X_{ee}(\mathbf{r}_{12})\ . \tag{2.29}$$

The structure function is easily obtained from Eq. (2.5).

Another interesting quantity is the spin structure factor defined by $S_\sigma(\mathbf{k})=\langle\rho^\dagger_{\sigma,\mathbf{k}}\rho_{\sigma,\mathbf{k}}\rangle$, with

$$\rho_{\sigma,\mathbf{k}}=\frac{1}{\sqrt{N}}\sum_i \exp(i\mathbf{k}\cdot\mathbf{r}_i)\sigma_z(i)\ ,$$

given by

$$S_\sigma(\mathbf{k})=1+\rho\sum_i \cos(\mathbf{k}\cdot\mathbf{r}_i)\{X_{ee}(\mathbf{r}_i)+N_{ee}(\mathbf{r}_i)\} +\delta(\mathbf{k}-\mathbf{Q})Nm^2\ . \tag{2.30}$$

The coherent term arises from separable cluster diagrams where the two external points are disconnected from each other and both are separability points. One can easily verify that the separability theorem does not apply here at $\mathbf{k}=\mathbf{Q}$, because of the presence of spin operator $\sigma_z(i)$ for each external point. The resulting expression is the product of the identical vertex corrections associated with the two external points. It is found that the vertex correction m coincides with the staggered magnetization discussed in the next subsection.

B. The FHNC scheme for $n(\mathbf{r}_{11'})$

The one-body density matrix is defined as

$$n(\mathbf{r}_{1,1'})=\sum_\sigma \xi^\dagger_\sigma(1')\hat{n}(1,1')\xi_\sigma(1)\ , \tag{2.31}$$

$$\hat{n}(1,1')=\frac{A}{\mathcal{N}}\sum_{\mathbf{r}_2\cdots\mathbf{r}_A}\Phi^\dagger_{\mathrm{SDW}}(12\ldots A) \times\prod_{i,j\neq 1,1'} f(r_{1'i})f(r_{1j}) \times\prod_{i<j\neq 1,1'} f^2(r_{ij})\Phi_{\mathrm{SDW}}(1'2\cdots A)\ . \tag{2.32}$$

If the correlation $f(\mathbf{r}_{ij})$ is set equal to 1, one gets the uncorrelated one-body density matrix $n(\mathbf{r}_{11'})=l_u(\mathbf{r}_{11'})$. More generally, the one-body density matrix is the u component of $\hat{n}(1,1')$. Its cluster expansion can be easily deduced from that given in Ref. 24 for a continuous system, following the procedure outlined in the previous subsection for $g(\mathbf{r}_{ij})$. One ends up with the result

$$\hat{n}(1,1')=\sum_p \rho^p \sum_{\mathbf{r}_2,\ldots,\mathbf{r}_p}\hat{\mathcal{L}}^{(p)}_n(1,1',\mathbf{r}_3,\ldots,\mathbf{r}_p)\ , \tag{2.33}$$

where $\hat{\mathcal{L}}^{(p)}_n(1,1',\mathbf{r}_3,\ldots,\mathbf{r}_P)$ is the sum of the linked, topologically distinct terms having two external indices (1 and 1') and $p-1$ internal indices. Each term is a product of dynamical and statistical correlations. The dynamical correlations having 1 or 1' as particle variable must be of the type $\xi(\mathbf{r})=f(\mathbf{r})-1$. As discussed in Ref. 24, the reducibilities in 1 and 1' cannot be removed and they appear as vertex corrections. The density matrix is given by

$$\hat{n}(1,1')=n_0\{(1/\nu)\hat{\rho}(1,1')-\hat{N}_{\xi c\xi c}(1,1') -\hat{E}_{\xi c\xi c}(1,1')\}e^{[N_{\xi\xi}(\mathbf{r}_{1,1'})+E_{\xi\xi}(\mathbf{r}_{1,1'})]}\ . \tag{2.34}$$

The FHNC equations for the vertex correction n_0, the chain functions $N_{\xi\xi}$, $N_{\xi d}$, $N_{\xi e}$ and the composite functions $X_{\xi\xi}$, $X_{\xi d}$, $X_{\xi e}$ coincide with those of the paramagnetic case[11] and will not be repeated here. To calculate the chain operator $\hat{N}_{\xi c\xi c}$, besides $\hat{N}_{\rho a}$, one similarly has to evaluate the chain operator $\hat{N}_{xa}(1,i)$ having $\hat{X}_{\xi c}$ as the first element of $\hat{N}_{xa}$:

$$\hat{N}_{xa}(1,i)=\hat{X}_{\xi cc}(1,i)-[\hat{X}_{\xi cc}(1,k)|(1/\nu)\hat{\rho}(k,i)] +\{\hat{N}_{xa}(1,k)|\hat{X}_{cc}(k,i)-[\hat{X}_{cc}(k,l)|(1/\nu)\hat{\rho}(l,i)]\}\ . \tag{2.35}$$

The chain operator $\hat{N}_{\xi c\xi c}(1,1')$ is then given by

$$\hat{N}_{\xi c\xi c}(1,1')=\{\hat{N}_{\rho a}(1,i)|\hat{X}_{cc\xi}(i,1') -[\hat{X}_{cc}(i,k)(1/\nu)\hat{\rho}(k,1')]\} +[\hat{X}_{\xi cc}(1,i)|\hat{N}_{a\rho}(i,1')] +[\hat{N}_{xa}(1,i)|\hat{X}_{cc\xi}(i,1')]\ , \tag{2.36}$$

where

$$\hat{X}_{\xi cc}(1,i)=[g_{\xi d}(\mathbf{r}_{1i})-1][\hat{N}_{\xi cc}(1,i)-\tfrac{1}{2}\hat{\rho}(1,i)] +g_{\xi d}(\mathbf{r}_{1i})\hat{E}_{\xi cc}(1,i)\ , \tag{2.37}$$

$$\hat{N}_{\xi cc}(1,i)=\{\hat{N}_{\rho a}(1,k)|\hat{X}_{cc}(k,i) -[\hat{X}_{cc}(k,l)|(1/\nu)\hat{\rho}(l,i)]\} +[\hat{X}_{\xi cc}(1,k)|\hat{N}_{a\rho}(k,i)] +[\hat{N}_{xa}(1,k)|\hat{X}_{cc}(k,i)] , \quad (2.38)$$

with $g_{\xi d}(\mathbf{r}_{1i})=\exp\{N_{\xi d}(\mathbf{r}_{1i})+E_{\xi d}(\mathbf{r}_{1i})\}$.

The staggered magnetization m, defined as

$$m=\frac{1}{N}\langle S_{\mathbf{Q}}^{z}\rangle=\left\langle \sum_{\mathbf{k}} c_{\mathbf{k}+\mathbf{Q},\alpha}^{\dagger}\sigma_{\alpha,\alpha'}^{\dagger}c_{\mathbf{k},\alpha'}\right\rangle \quad (2.39)$$

can also be calculated within the FHNC scheme. In fact, it is related to $\hat{n}(11')$ by the equation

$$m=\frac{1}{N}\sum_{\mathbf{r}_1} e^{i\mathbf{Q}\cdot\mathbf{r}_1}[n_{\uparrow}(r_{11'}=0)-n_{\downarrow}(r_{11'}=0)] , \quad (2.40)$$

where $n_{\sigma}(r_{11'})=\xi_{\sigma}^{\dagger}(1')\hat{n}(1,1')\xi_{\sigma}(1)$. In the paramagnetic case $m=0$ since $n_{\uparrow}=n_{\downarrow}$.

The u part of $n(1,1')$ does not contribute, because it does not depend upon σ. One gets the result

$$m=\nu n_{v}(\mathbf{r}_{11'}=0) . \quad (2.41)$$

For the uncorrelated model, $n_v(0)=(1/\nu)l_v(0)$ and one recovers $\Delta=Um/2$.[7]

III. OLD FHNC/n AND NEW FHNC-n SCHEMES

We have shown that $g(\mathbf{r}_{12})$ and $n(\mathbf{r}_{11'})$ can be expressed in terms of the nodal and composite functions $N_{\alpha\beta}$ and $X_{\alpha\beta}$. These functions are calculated by solving a set of integral equations, which, in principle, depend upon the dynamical correlations $h(\mathbf{r}_{ij})$ and $\xi(\mathbf{r}_{ij})$ and the uncorrelated density matrix $\hat{\rho}(i,j)$ only. However, no closed formulation exists for the functions $E_{\alpha\beta}(\mathbf{r}_{ij})$ corresponding to the elementary diagrams. As a result, $E_{\alpha\beta}(\mathbf{r}_{ij})$ are approximated by expressions which include only a subset of elementary diagrams. Therefore, the associated FHNC scheme is not exact.

A commonly used approximation scheme for the functions $E_{\alpha\beta}$ is the so-called FHNC/n scheme, which consist of expressing $E_{\alpha\beta}$ as a series

$$E_{\alpha\beta}(\mathbf{r}_{ij})=\sum_{l}(\mathscr{E}_{l})_{\alpha\beta}(\mathbf{r}_{ij}) , \quad (3.1)$$

where the index l is the number of points of the irreducible elementary diagram (IED) $\mathscr{E}_{\alpha\beta}$ of type $\alpha\beta$. An IED is an elementary diagram with no pairs of reducibility points. [A pair (ij) of reducibility points is defined by the property that a cut of the diagram through the points i and j will produce two diagrams, one of which is a two point ij diagram.] For instance, Fig. 2(a) is irreducible, whereas Figs. 2(b) and 2(c) are reducible (see the Appendix for more details). In the FHNC/n scheme the bonds of the IED included are given by pair distribution functions

$$g_{\alpha\beta}=\delta_{dd,\alpha\beta}+N_{\alpha\beta}+X_{\alpha\beta}-(1/\nu)\hat{\rho}\delta_{cc,\alpha\beta} ,$$

therefore, $(\mathscr{E}_m)_{\alpha\beta}$ are functionals of $-(1/\nu)\hat{\rho}$, $N_{\alpha\beta}$, and

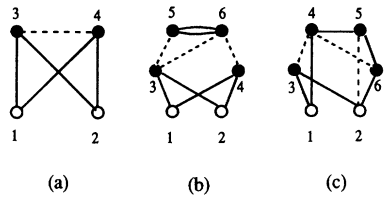

FIG. 2. The example of reducible and irreducible elementary diagrams.

$X_{\alpha\beta}$. The explicit expressions of the functionals $(\mathscr{E}_4)_{\alpha\beta}$ can be found in Ref. 11.

If $E_{\alpha\beta}$ is taken to be zero, the corresponding approximation is called FHNC/0. Similarly, the approximation FHNC/n is obtained by truncating the series (3.1) at $l=n$.

Both the FHNC/0 and FHNC/4 approximations have been used in Ref. 11 to study the 1D Hubbard model with a Jastrow correlated paramagnetic state ($\Delta=0$). It has been shown that inclusion of the four-body elementary diagrams can provide only very small corrections to the sum-rule violation and even smaller correction to E/Nt up to $U/t=5$. For larger U/t and/or $\Delta>0$, the FHNC/n scheme does not seem to be work at all.

An alternative scheme can be obtained by a different grouping of $E_{\alpha\beta}$, according to the number of factors $h(\mathbf{r}_{ij})$ and $\xi(\mathbf{r}_{ij})$. In this case, $E_{\alpha\beta}$ are given by

$$E_{\alpha\beta}(\mathbf{r}_{ij})=\sum_{l}E_{\alpha\beta}^{(l)}(\mathbf{r}_{ij}) , \quad (3.2)$$

where $E_{\alpha\beta}^{(l)}$ are not necessarily IED's, in contrast to Eq. (3.1), and the suffix l denotes the number of dynamical correlation factors appearing in the diagrams. The scheme FHNC-n consists of truncating the series (3.2) at $l=n$. The $E_{\alpha\beta}^{(l\leq 3)}$ elementary diagrams are discussed in the Appendix.

This scheme shares some of the special features of the PS cluster expansion, in which the full $g(\mathbf{r}_{12})$ [or $\hat{n}(1,1')$] is given by an expression like Eq. (3.2). The main feature of the PS expansion is that at each order of PS there is no Pauli principle violation, so that the various sum rules are exactly fulfilled.

In the case of the Gutzwiller correlation operator, the PS expansion leads to the following expressions for the pair function, the one-body density matrix, and the energy per particle:

$$g(\mathbf{r}=0)=g^2\sum_{k=1}^{\infty}C_g^k(0)(g^2-1)^{k-1} , \quad (3.3)$$

$$g(\mathbf{r}\neq 0)=\sum_{k=1}^{\infty}[C_g^k(\mathbf{r})](g^2-1)^{k-1} , \quad (3.4)$$

$$\hat{n}(1,1')=\sum_{k,l=0}^{\infty}\hat{C}_n^{kl}(11')(g-1)^k(g^2-1)^l , \quad (3.5)$$

$$\frac{E_0}{Nt}=-z\rho\sum_{k,l=0}^{\infty}C_{nu}^{kl}(\mathbf{a})(g-1)^k(g^2-1)^l +\frac{1}{2}\frac{U}{t}\rho^2g^2\sum_{k=1}^{\infty}C_g^k(0)(g^2-1)^{k-1} . \quad (3.6)$$

Here, the functions $C_g^k(\mathbf{r})$ and $\hat{C}_n^{kl}(11')$ are obtained by calculating the g diagrams with k h lines and the $\hat{n}$ diagrams with k ξ and l h lines, respectively. The multidimensional integrations in the calculations of the g and $\hat{n}$ diagrams are simplified by the property that the Gutzwiller correlation is strictly on site. In a given diagram, the integration over a variable x_i leads to a contraction of all the dynamical lines reaching the point i to the single point i itself and to a factor $\rho(g-1)^k(g^2-1)^l$, where k is the number of $\xi(\mathbf{r}_{ij})$ lines and l that of $h(\mathbf{r}_{ij})$ lines. For instance, the diagrams in the first row of Fig. 1 for $\Delta=0$ give rise to $(g^2-1)^2\rho\delta(\mathbf{r}_{12})$, $(g^2-1)\rho L_2(\mathbf{r}_{12})$, $-(1/\nu)(g^2-1)^2\rho^2 L_3(\mathbf{r}_{12})$, and $-(1/\nu)(g^2-1)\rho L_1(\mathbf{r}_{12})$, where L_1 and L_2 and L_3 correspond to the reduced diagrams shown in Table I. A close analysis of the cluster diagrams and the cancellations existing among them shows[25] that the coefficients have the following structure:

$$\begin{aligned} &C_g^k(\mathbf{r})=\alpha^k(\mathbf{r},\rho)\rho^{k-1}\,, \\ &C_n^{kl}(\mathbf{r}=0)=\beta^{kl}(\rho)\rho^{k+l-1}+\gamma^{kl}(0,\rho)\rho^{k+l}\,, \\ &C_n^{kl}(\mathbf{r}\neq 0)=\gamma^{kl}(\mathbf{r},\rho)\rho^{k+l}\,, \end{aligned} \tag{3.7}$$

where the functions α, β, and γ are obtained by integrating reduced diagrams over the internal points, each integration carrying an extra factor ρ. The explicit expressions of α, β, and γ entering in the PS$^{(3)}$ approximation for $\Delta=0$ are given by

$$\begin{aligned} &\alpha^1(\mathbf{r},\rho)=1+L_2(\mathbf{r},\rho)\,,\quad \alpha^2(\mathbf{r},\rho)=L_2(\mathbf{r},\rho)+\tfrac{1}{2}L_3(\mathbf{r},\rho)\,, \\ &\alpha^3(\mathbf{r},\rho)=-\tfrac{3}{4}L_2(\mathbf{r},\rho)+\tfrac{1}{4}L_4(\mathbf{r},\rho)-\tfrac{1}{2}L_7(\mathbf{r},\rho)+3L_9(\mathbf{r},\rho)-3L_{16}(\mathbf{r},\rho)\,, \\ &\alpha^4(\mathbf{r},\rho)=[(\tfrac{3}{4}-\tfrac{1}{2}L_3(0,\rho)]L_2(\mathbf{r},\rho)-\tfrac{1}{4}L_3(\mathbf{r},\rho)-\tfrac{1}{4}L_4(\mathbf{r},\rho)+\tfrac{1}{8}L_5(\mathbf{r},\rho) \\ &\qquad +L_7(\mathbf{r},\rho)-5L_9(\mathbf{r},\rho)-2L_{10}(\mathbf{r},\rho)+6L_{14}(\mathbf{r},\rho)+L_{15}(\mathbf{r},\rho) \\ &\qquad +3L_{16}(\mathbf{r},\rho)-3L_{17}(\mathbf{r},\rho)+L_{18}(\mathbf{r},\rho)+4L_{19}(\mathbf{r},\rho)-8L_{20}(\mathbf{r},\rho)\,, \end{aligned} \tag{3.8}$$

and

$$\begin{aligned} &\gamma^{00}(\mathbf{r},\rho)=-\nu L_1(\mathbf{r},\rho)\,,\quad \gamma^{10}(\mathbf{r},\rho)=-2\gamma^{01}(\mathbf{r},\rho)=-\nu L_1(\mathbf{r},\rho)\,,\quad \gamma^{20}(\mathbf{r},\rho)=-\tfrac{1}{2}[L_1(\mathbf{r},\rho)-L_6(\mathbf{r},\rho)]\,, \\ &\gamma^{11}(\mathbf{r},\rho)=-2\gamma^{02}(\mathbf{r},\rho)=2L_1(\mathbf{r},\rho)+L_8(\mathbf{r},\rho)\,,\gamma^{21}(\mathbf{r},\rho)=\tfrac{3}{4}L_1(\mathbf{r},\rho)-\tfrac{3}{4}L_6(\mathbf{r},\rho)-\tfrac{1}{2}L_8(\mathbf{r},\rho)+L_{11}(\mathbf{r},\rho)\,, \\ &\gamma^{12}(\mathbf{r},\rho)=-2\gamma^{03}(\mathbf{r},\rho)=[-\tfrac{5}{2}+L_3(0,\rho)]L_1(\mathbf{r},\rho)-\tfrac{5}{2}L_8(\mathbf{r},\rho)+2L_{12}(\mathbf{r},\rho)\,, \end{aligned} \tag{3.9}$$

$$\beta^{20}=-\gamma^{02}(0,\rho)\,,\quad \beta^{21}=-\gamma^{03}(0,\rho)\,. \tag{3.10}$$

In the 1D case,

$$L_1(r_{12},\rho)=-\frac{1}{\nu}\sum_{|k|<k_F}\varphi^\dagger(r_1)\varphi(r_2)=\frac{1}{\nu}\frac{\sin(k_F r_{12})}{k_F r_{12}}$$

with $k_F=\pi\rho/\nu a$, one can easily obtain the analytical expressions of the functions $L_{n\le 19}$.[26] The values of $L_{n\le 19}(0,\rho)$ and $\bar{L}_{n\le 19}(k=0)$ entering the $C_g(0)$ coefficients are listed in Table I, and the values of $L_i(a,\rho)$ $(i=1,6,8,11,12)$ entering the coefficients $C_n(r=a)$ are given by

$$\begin{aligned} &L_1(a,\rho)=-\frac{\sin(k_F a)}{\nu k_F a}\,,\quad L_6(1)=-\nu^2 L_1^3(1)\,,\quad L_8(a,\rho)=\frac{(k_F^2+1)\sin(k_F a)-k_F\cos(k_F a)}{2\nu(k_F a)^3}\,, \\ &L_{11}(a,\rho)=\frac{[\sin(k_F a)-2k_F a]\sin(k_F a)}{2\nu^2(k_F a)^4}\,,\quad L_{12}(a,\rho)=\frac{4(k_F a)^2\sin(k_F a)-2k_F a\cos(k_F a)-2\sin(a,\rho)}{12\nu^2(k_F a)^3}\,. \end{aligned} \tag{3.11}$$

One can easily check that sum rules (2.7) and (2.8) are exactly satisfied at each of the three PS orders, irrespective of dimensionality. The coefficients for $g(0)$ and $n(a)$ coincide with the corresponding ones obtained by Metzner and Vollhardt in their cluster analysis.[18]

In the 1D case, scaling considerations[25] imply that the density dependence of α is simply given by $\alpha(\mathbf{r},\rho)=\alpha(k_F r)$ and similarly, $\beta(\rho)=\beta$ and $\gamma(\mathbf{r},\rho)=\gamma(k_F r)$. Therefore, the density dependence of C_g and C_n is the same as that found by Metzner and Vollhardt, and allows for exact analytical expressions for $C_g(0)$ and $c_{nu}(a)$, once particle-hole symmetry is used.[18] Similar expressions for the coefficients C_g and $\hat{C}_n$ entering the PS$^{(3)}$ approximation can be easily found for the case $\Delta\neq 0$.

The FHNC-n scheme adds many-body cluster contributions to the PS$^{(n)}$ approximation by using FHNC theory. More precise, the FHNC equations derived in Sec. II are solved by approximating the functions $E_{\alpha\beta}$ according to Eq. (3.2). This guarantees that all the diagrams of PS$^{(n)}$ are included, as well as all the many-body cluster diagrams needed to get a realistic estimate of

E/Nt.

It should be noted that the large amount of Pauli principle violation introduced in the FHNC/n scheme by the $\mathcal{E}_n$ diagrams can be completely cancelled only after considering higher-order IED $\mathcal{E}_{m>n}$. By contrast, in the FHNC-n scheme, the elementary diagrams $E^{(n)}$ exactly cancel these spurious effects of unphysical diagrams up to order n.

There are important technical differences between the FHNC/n and FHNC-n schemes, which are worth mentioning. The $\mathcal{E}_4$ diagrams in FHNC/4 give rise to 83 functions, and the number of $\mathcal{E}_5$ diagrams is so large that no calculation exists in the FHNC/5 approximation. On the contrary, the first three powers of FHNC-n theory can be easily handled within the present numerical capabilities. For instance, in the first order of FHNC-n theory, $E_{dd}^{(1)}=E_{de}^{(1)}=\hat{E}_{cc}^{(1)}=0$ and $E_{ee}^{(1)}$ is given by [see Fig. 2(a)]

$$E_{ee}^{(1)}(\mathbf{r}_{34})=2\rho^2\sum_{\mathbf{x}_3\mathbf{x}_4}\left[-\frac{1}{\nu}\hat{\rho}(1,3)\right]\left[-\frac{1}{\nu}\hat{\rho}(3,2)\right]\left[-\frac{1}{\nu}\hat{\rho}(2,4)\right]\left[-\frac{1}{\nu}\hat{\rho}(1,4)\right]h(\mathbf{r}_{34})\,, \tag{3.12}$$

which coincides with one of the $(\mathcal{E}_4)_{ee}$ elementary diagrams. In the second- and third-order approximations, E_{dd} still vanishes and E_{de}, E_{ee}, and $\hat{E}_{cc}\neq 0$ (Fig. 3). However, the FHNC-n scheme requires the evaluation of integrals in high dimension. For instance, the $E^{(2)}$ diagrams imply up to four-dimensional integrals and $E^{(3)}$ up to six-dimensional integrals. They can be evaluated by using Monte Carlo procedures. In the case of the Gutzwiller correlation operator, the integration are obviously simplified with respect to the Jastrow case and analytical expressions of can be found for $E_{\alpha\beta}$.

IV. RESULTS

The PS$^{(3)}$ approximation and the FHNC/n and FHNC-n schemes have been applied to calculate the ground-state properties of the 1D Hubbard model, with the Gutzwiller correlated SDW trial functions. The Gutzwiller strength g and the uncorrelated gap Δ have been used as the only parameters of the theory.

Table II gives the results of the first three orders of PS for E/Nt with $U/t=4$, calculated at four different values of the gap parameter Δ and the values of g given by Yokoyama and Shiba, in correspondence with the minimum of E/Nt. A minimum of E/Nt is found at each order of the PS expansion; the minima found for the paramagnetic case ($\Delta=0$) and the more general SDW

TABLE I. The reduced diagrams and their values at $x=0$ and $k=0$ in the 1D paramagnetic case.

Diagrams	L_i	$x=0$	$k=0$	Diagrams	L_i	$x=0$	$k=0$
	L_1	$-\frac{1}{\nu}$	-1		L_{11}	$-\frac{2}{3\nu^2}$	$-\frac{7}{12\nu}$
	L_2	$-\frac{1}{\nu}$	-1		L_{12}	$\frac{1}{2\nu^2}$	$\frac{7}{12\nu}$
	L_3	$\frac{2}{3\nu}$	1		L_{13}	$-\frac{1}{2\nu^3}$	$-\frac{1}{2\nu^2}$
	L_4	$-\frac{1}{2\nu}$	-1		L_{14}	$\frac{9}{20\nu^2}$	$\frac{2}{3\nu}$
	L_5	$\frac{2}{5\nu}$	1		L_{15}	$-\frac{1}{2\nu^3}$	$-\frac{2}{3\nu}$
	L_6	$-\frac{1}{\nu}$	$-\frac{3}{4}$		L_{16}	$\frac{11}{30\nu^3}$	$\frac{2}{3\nu^2}$
	L_7	$-\frac{1}{\nu}$	$-\frac{2}{3}$		L_{17}	$\frac{2}{5\nu^3}$	$\frac{1}{2\nu^2}$
	L_8	$\frac{2}{3\nu}$	$\frac{3}{4}$		L_{18}	$-\frac{9}{20\nu^3}$	$-\frac{1}{2\nu^2}$
	L_9	$-\frac{2}{3\nu^2}$	$-\frac{2}{3\nu}$		L_{19}	$-\frac{11}{30\nu^4}$	$-\frac{1}{2\nu^3}$
	L_{10}	$-\frac{2}{3\nu^2}$	$-\frac{1}{2\nu}$				

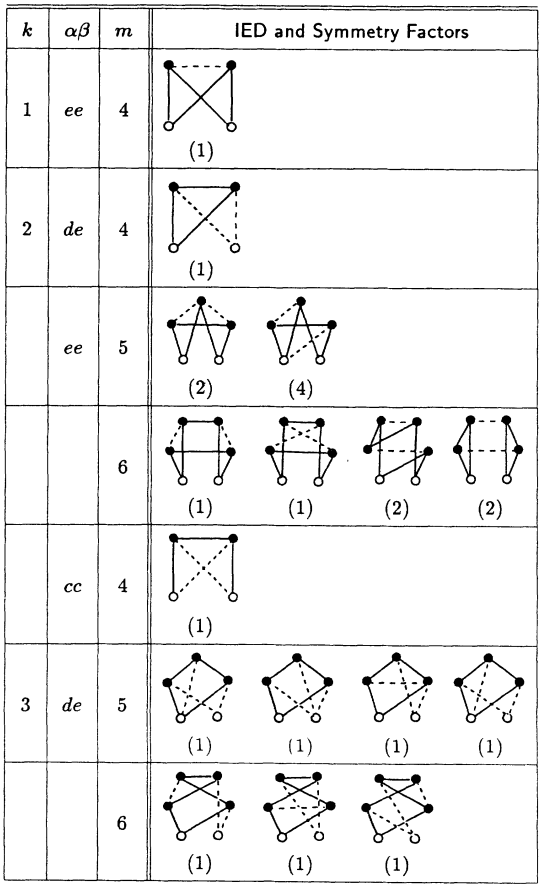

FIG. 3. The irreducible elementary diagrams $(\mathcal{E}_m)_{\alpha\beta}$ for $E_{\alpha\beta}^{(1)}$, $E_{\alpha\beta}^{(2)}$, and $E_{de}^{(3)}$, and their symmetry factors.

case ($\Delta \neq 0$) are listed in Table III. In the 2D case, for the Gutzwiller correlation operator, $PS^{(2)}$ coincides with the approximation suggested by Carmelo *et al.*[27]

Table IV reports the results of the FHNC/0, FHNC/4, FHNC-2, and FHNC-3 approximations for E/Nt with $U/t=4$, compared with the VMC results obtained by Yokoyama and Shiba. The minima for E/Nt in FHNC/0, FHNC/4, FHNC-2, and FHNC-3 are given in Table V, where no result is reported for FHNC/n at $\Delta \neq 0$ because in that case no minima have been found.

The PS and FHNC/n results represented in Tables II–V suggest the following comments: (i) the third order of PS is a very good approximation in the weak-coupling regime ($g \geq 0.7$) irrespective of the value of Δ. (ii) The FHNC/0 and FHNC/4 schemes provide very good results for small values of Δ ($\Delta \approx 0$), also in the strongly interacting regime ($g \geq 0.4$). They, however, begin to break down for $\Delta \geq 2$; in particular, no minimum is found for E/Nt as a function of Δ for $U/t \geq 4$. (iii) The optimal trial wave functions have both strong SDW and Gutzwiller correlations. For instance, for $U/t=4$, at a minimum of E/Nt (which is close to within 10% to the VMC result), we find $\Delta=0.3$ and $g=0.5$. As expected, the correlations sensibly reduce the value of the gap parameter which optimizes E/Nt. (The MF value of Δ for $U/t=4$ at $\rho=1$ is $\Delta \approx 1.55$). (iv) The FHNC-3 estimate compares very well with the VMC data, as also shown in Fig. 4 for $U/t=4$. Results of the same, or even better quality, are obtained for other values of $U/t \leq 8$.

The FHNC-n scheme, being a compromise between the PS and the FHNC summations, yields reasonable results for both energy, and sum rules. It is clearly superior to the FHNC/n scheme, where statistical correlations are strong.

It turns out that the sum rule $S(0)=0$ is very well satisfied at the second and third orders of the FHNC-n scheme as seen from Table VI and the sum rule $n(0)=1/\nu$ is almost exactly fulfilled in the FHNC-3 approximation as shown in Table VII. The full density-density correlation function $S(\mathbf{k})$ is plotted in Fig. 5 at various values of Δ.

The momentum distribution $n(\mathbf{k})$ calculated for half-filling is shown in Fig. 6 at $g=0.5$ and various values of Δ and in Fig. 7 at $\Delta=0.3$ and various values of g. The Jastrow correlations do not change the main behavior of the uncorrelated momentum distribution. At $\Delta=0$, the discontinuity at $k=k_F$ persists although it is reduced by a factor depending upon g and it is $\sim 10\%$ for $g=0.5$. In the case of the SDW reference state, the Fermi jump disappears and the correlation shrinks the shapes of $n(k)$, as can be seen in Fig. 6 and the momentum distribution corresponding to the best variational bounds ($g=0.5$, $\Delta \approx 0.3$) seems to be the closest to $n(k)$ obtained in quantum Monte Carlo by Sorella *et al.*[3]

Finally, we have calculated the single-particle spectrum $\epsilon(\mathbf{k})$ by the procedure of Ref. 11. To this aim, we have evaluated the expectation value of the Hamiltonian $E(\alpha,\mathbf{p})/Nt$ as described in Sec. II by using the following exchange operator:

$$\hat{\rho}_{\mathbf{p}}(i,j)=\hat{\rho}(i,j)+\alpha \hat{f}_{\mathbf{p}}(i,j) , \tag{4.1}$$

instead of $\hat{\rho}(i,j)$, where

$$\begin{aligned} f^{u}_{\mathbf{p}}(\mathbf{r}_{12}) &= [v^2(\mathbf{p})+u^2(\mathbf{p})\cos(\mathbf{Q}\cdot\mathbf{r})]\cos(\mathbf{p}\cdot\mathbf{r}) \\ &\quad -[u^2(\mathbf{k}_F)+v^2(\mathbf{k}_F)\cos(\mathbf{Q}\cdot\mathbf{r})]\cos(\mathbf{k}_F\cdot\mathbf{r}) , \\ f^{v}_{\mathbf{p}}(\mathbf{r}_{12}) &= -[v(\mathbf{p})u(\mathbf{p})\cos(\mathbf{p}\cdot\mathbf{r}) \\ &\quad +u(\mathbf{k}_F)v(\mathbf{k}_G)\cos(\mathbf{k}_F\cdot\mathbf{r})][1+\cos(\mathbf{Q}\cdot\mathbf{r})] . \end{aligned} \tag{4.2}$$

The quantity

$$\epsilon(\mathbf{p})=\frac{d}{d\alpha}\{E(\alpha,\mathbf{p})/Nt\}|_{\alpha=0} \tag{4.3}$$

gives the excitation energy of the correlated particle-hole state $\hat{F}|\Phi_{\mathrm{SDW}}(\mathbf{p},\mathbf{h}=\mathbf{k}_F)\rangle$, obtained by substituting in Φ_{SDW} the hole state $\psi_{k_F\sigma}$, given by Eq. (1.4), with the particle state

$$\psi_{\mathbf{p}\sigma}(r_i)=[v(\mathbf{p})e^{i\mathbf{p}\cdot\mathbf{r}_i}-\hat{\sigma}_z(i)u(\mathbf{k})e^{i(\mathbf{p}+\mathbf{Q})\cdot\mathbf{r}_i}]\xi_\sigma(i) . \tag{4.4}$$

The state $\hat{F}|\Phi_{\mathrm{SDW}}(\mathbf{p},\mathbf{h}=\mathbf{k}_F)\rangle$ is orthogonal to $\hat{F}|\Phi_{\mathrm{SDW}}\rangle$ for momentum conservation. For $p=k_F$, $\epsilon(k_F)$ has a jump, representing the gap $\bar{\Delta}$ of the single-particle excitation spectrum.

TABLE III. The energy upperbound of the 1D Hubbard model with $U/t=4$ by using MF, first, second, and third PS approximations and the VMC (Ref. 10) for paramagnetic and antiferromagnetic cases, respectively.

	MF	First	Second	Third	VMC
$\Delta=0$	−0.27	−0.39	−0.44	−0.47	−0.52
g	1.0	0.65	0.60	0.55	0.45
$\Delta\neq 0$	−0.47	−0.49	−0.51	−0.52	−0.54
Δ/g	1.54/1.0	0.95/0.75	0.70/0.65	0.40/0.575	0.3/0.5

TABLE II. E/Nt for the 1D Hubbard model with $U/t=4$ at $\rho=1$ by using MF, first, second, and third PS approximations given at four different values of Δ. The last column is the VMC results from Ref. 10.

Δ	g	MF	First	Second	Third	VMC
0.0	0.45	−0.27	−0.36	−0.41	−0.45	−0.52
0.3	0.5	−0.33	−0.42	−0.48	−0.52	−0.54
0.6	0.6	−0.40	−0.47	−0.51	−0.52	−0.53
0.9	0.7	−0.44	−0.49	−0.50	−0.50	−0.51

TABLE IV. E/Nt for the 1D Hubbard model with $U/t=1$ at $\rho=1$ by using MF, FHNC/0, FHNC/4, FHNC-2, and FHNC-3 approximations given at four different values of Δ. The last column is the VMC results from Ref. 10.

Δ	g	FHNC/0	FHNC/4	FHNC-2	FHNC-3	VMC
0.0	0.45	−0.51	−0.51	−0.44	−0.51	−0.52
0.3	0.5	−0.59	−0.51	−0.49	−0.54	−0.54
0.6	0.6	−0.66	−0.54	−0.50	−0.52	−0.53
0.9	0.7	−0.71	−0.55	−0.50	−0.51	−0.51

TABLE V. The energy upperbound of the 1D Hubbard model with $U/t=4$ by using MF, FHNC/0, FHNC/4, FHNC-2, and FHNC-3 approximations and the VMC (Ref. 10) for paramagnetic and antiferromagnetic cases, respectively.

	FHNC/0	FHNC/4	FHNC-2	FHNC-3	VMC
$\Delta=0$	−0.52	−0.52	−0.45	−0.51	−0.52
g	0.5	0.5	0.55	0.45	0.45
$\Delta\neq 0$			−0.52	−0.54	−0.54
Δ/g			0.7/0.6	0.325/0.5	0.3/0.5

TABLE VI. $S(0)$ in FHNC/0, FHNC/4, FHNC-2, and FHNC-3 approximations for various values of Δ and g.

g	Δ	FHNC/0	FHNC/4	FHNC-2	FHNC-3
	0.0	−0.149	−0.057	0.015	0.013
0.7	0.4	−0.170	−0.088	0.018	0.010
	0.8	−0.206	−0.141	0.017	0.016
	0.0	−0.170	−0.132	0.049	0.013
0.4	0.4	−0.210	−0.133	0.021	0.007
	0.8	−0.267	−0.182	0.094	−0.055

In the uncorrelated case, $\bar{\Delta}\equiv\Delta$. We found that $\bar{\Delta}$ is marginally smaller than the gap parameter Δ owing to correlation. At $U/t=4$ and half-filling, $\bar{\Delta}=0.26$ while $\Delta=0.3$. The staggered magnetization m given by Eq. (2.41) reduces to 0.54 as compared with the MF value $m_{\rm MF}\approx 0.77$ for $U/t=4$ at half-filling. These values of gap parameter Δ and of magnetization m coincide with those obtained by the VMC calculation.[10] The corresponding uncorrelated SDW gap in a simple Hartree-Fock is $\Delta_{\rm MF}=\bar{\Delta}_{\rm MF}=1.54$.

It is very surprising to find that the correlation-induced reduction of gap $\bar{\Delta}$ is so much larger ($\bar{\Delta}/\bar{\Delta}_{\rm MF}=0.19$) than the corresponding reduction of magnetization ($m/m_{\rm MF}=0.69$). In the true ground state, just the opposite is expected. We know from the exact Lieb-Wu solution[17] that $m_{\rm LW}=0$ for all U, and that $\bar{\Delta}_{\rm LW}=0.64$ for $U/t=4$.[28]

Of course, a nonzero value of m is an intrinsic property of any correlated SDW wave function, and is neither worrying nor surprising. The magnetic solitons which destroy the global antiferromagnetic long-range order parameter in the exact case are simply not allowed in the SDW state, no matter how much further correlation is added. Still, we would expect the correlated SDW state to represent a reasonable description of the local physical state, so to speak, between two consecutive solitons.

The excessive reduction of Δ and $\bar{\Delta}$ to values severely below the exact $\Delta_{\rm LW}$ is a negative feature of the Gutzwiller correlated SDW wave function, which appears to be more serious. At the moment, we can provide the following qualitative arguments about its origin. In our wave function, we have omitted direct electron-hole ($e-d$) attractive correlations, also called "excitonic correlation." Actually, it was shown in our earlier study[11] that $e-d$ correlations are of crucial importance when starting from the gapless paramagnetic Fermi sea. This suggested envisaging the true gap $2\bar{\Delta}_{\rm LW}$ as representing the effective exciton binding energy, and the true ground state as an excitonic insulator. The need for explicit $e-d$ correlations is less obvious in the present correlated SDW case. Here, a single-particle gap 2Δ is provided by the magnetic order parameter, and therefore excitons are not necessarily needed for the establishment of an insulating ground state at half-filling. Our finding that $\bar{\Delta}\ll\bar{\Delta}_{\rm LW}$, however, suggests that neglect of $e-d$ correlations is in some sense an oversimplification, even in the correlated SDW case. Based on these considerations, we would expect that including $e-d$ effects (for example, in the form of "quartet" correlations, as in Ref. 11) should reestablish $\bar{\Delta}\geq\bar{\Delta}_{\rm LW}$. Alternatively, our results imply that the CBF perturbative correction $\delta\Delta$ to the "variational" estimate $\bar{\Delta}$ must be greater than 0. This is a peculiar predicted feature of CBF perturbation theory for this case, since, based on the earlier calculations in continuous system,[4] one would have argued that $\delta\Delta<0$.

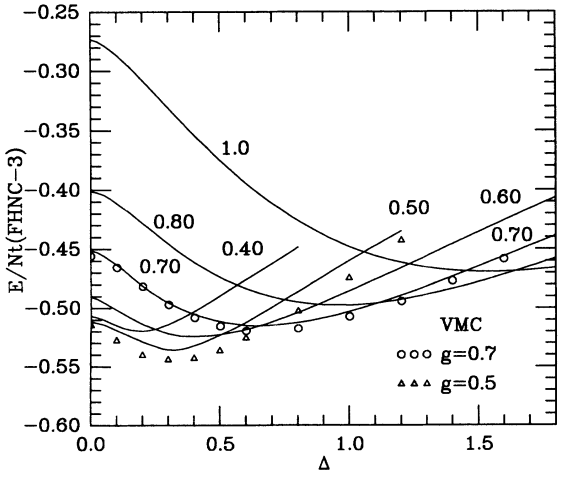

FIG. 4. The variational energy E/Nt in the FHNC-3 approximation compared with the VMC results at $U/t=4$ and $\rho=1$.

V. DISCUSSION AND CONCLUSION

The FHNC theory has been applied to study correlated SDW functions. A set of 10 coupled integral equations has been derived, whose solution allows the calculation of the pair distribution function, the one-body density matrix, and, consequently, the expectation value of the energy and other important quantities, such as the structure factor, the momentum distribution, the staggered magne-

TABLE VII. $n(0)$ in FHNC/0, FHNC/4, FHNC-2, and FHNC-3 approximations for various values of Δ and g.

g	Δ	FHNC/0	FHNC/4	FHNC-2	FHNC-3
	0.0	0.497	0.503	0.499	0.502
0.7	0.4	0.493	0.507	0.494	0.502
	0.8	0.489	0.510	0.488	0.500
	0.0	0.494	0.504	0.501	0.497
0.4	0.4	0.481	0.513	0.489	0.496
	0.8	0.469	0.523	0.473	0.489

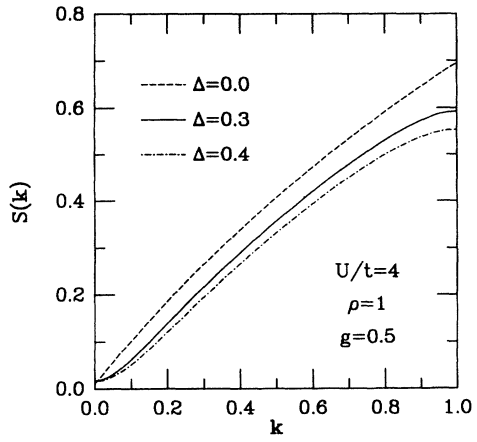

FIG. 5. The density-density correlation function $S(\mathbf{k})$ for the 1D Hubbard model with Gutzwiller correlated SDW functions.

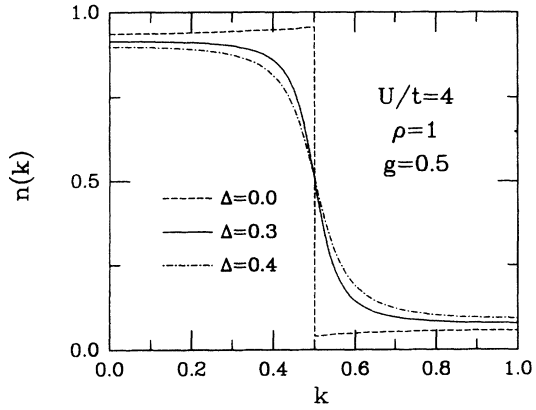

FIG. 6. The momentum distribution $N(\mathbf{k})$ for the 1D Hubbard model with Gutzwiller correlated SDW for $g=0.5$.

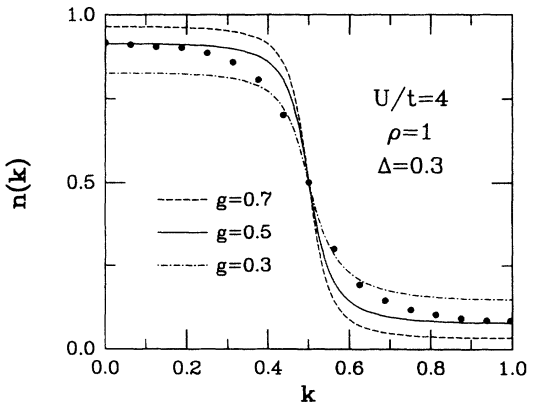

FIG. 7. The momentum distribution $n(\mathbf{k})$ for the 1D Hubbard model with Gutzwiller correlated SDW for $\Delta=0.3$. The solid dots denote the results obtained from quantum Monte Carlo (Ref. 3).

tization, etc.

A peculiarity of the FHNC theory for SDW's is that the *cc* quantities must be expressed in terms of two-component operators and that the ordering of such operators in a given cluster term is important. That is handled exactly by the FHNC equations.

The theory, in principle, depends only upon the dynamical correlations $h(\mathbf{r})$, $\xi(\mathbf{r})[h(\mathbf{r})=\xi^2(\mathbf{r})+2\xi(\mathbf{r})]$, and the operator $-(1/\nu)\hat{\rho}$ determined by the function $u(\mathbf{k})$ and $v(\mathbf{k})$ of the SDW reference state. However, the FHNC equations cannot be solved exactly because the expressions giving the sum of the elementary diagrams $E_{\alpha\beta}$ as functionals of $N_{\alpha\beta}$ and $X_{\alpha\beta}$ are not known. Therefore, one has to devise a proper FHNC approximation scheme, where certain classes of elementary diagrams are summed.

It is shown that the commonly used FHNC/n scheme is not suitable to deal with the correlated SDW state because the statistical correlations, namely, those already included in the SDW reference state through $\hat{\rho}$, get abnormally stronger and stronger as Δ increases. As a consequence, at the first two orders of such a scheme (FHNC/0 and FHNC/4), the sum rules $S(0)=0$ and $n(0)=1/\nu$ are badly violated and no minimum of E/Nt can really be found. The alternative possibility of a PS expansion has also been analyzed with the results that a minimum of E/Nt can always be found at each of the first three orders. Finally, we have presented a scheme, the FHNC-n scheme, where classes of elementary diagrams are summed up according to the PS expansion.

Our numerical analysis has been limited to the 1D Hubbard model with the Gutzwiller correlation operator for the sake of comparison with the existing VMC calculation. It, however, can be extended to treat the Jastrow correlation operator as well. It has been found that FHNC-3 leads to extremely good results for both E/Nt and the sum rules $S(0)=0$ and $n(0)=1/\nu$. The FHNC-2 approximation can safely be used in the process of minimizing E/Nt. A more detailed numerical application of FHNC-3 theory will be given for the 2D Hubbard model in a forthcoming paper.[29]

ACKNOWLEDGMENTS

We are grateful to S. Sorella for his help in calculating the Lieb-Wu gap, and to P. Fazekas for his interest. This work has been carried out under the partial sponsorship of the Italian National Institute for the Physics of Matter (INFM), of the CINECA Supercomputing Center, Casalecchio, and the European Research Office, U.S. Army.

APPENDIX: ELEMENTARY DIAGRAM IN THE FHNC-n SCHEME

The elementary diagrams entering in the FHNC-n scheme are all those having a number $k \leq n$ of dynamical correlation lines, namely, h or ξ lines. (See Fig. 2.) The most convenient way to construct the elementary diagrams $E^{(k)}_{\alpha\beta}$ is to first select the so-called irreducible elementary diagrams. These diagrams are defined as an elementary diagram having no pairs of reducibility points.

A pair of reducible points (ij) is such that a cut of the connection line between them will give rise to two separate parts of which one is an ij subdiagram. [Figure 2(a) is irreducible, where Figs. 2(b) and 2(c) are reducible; in Fig. 2(c), (24) is a pair of reducible points.]

It follows that any IED is the lowest-order diagram of a whole family of elementary diagrams having the same topology. In fact, one can substitute an ij bond of IED with a proper correlation function $g_{\alpha\beta}(\mathbf{r}_{ij})$.

Therefore, once we have all the IED's of order $k \leq n$, we can easily construct the rest of the elementary diagrams. For instance, Fig. 2(b) is obtained from Fig. 2(a) by replacing the $h(\mathbf{r}_{34})$ bond with $N_{dd}(\mathbf{r}_{34})$, as well as Fig. 2(c) is obtained from Fig. 2(a) by replacing $\hat{\rho}(4,2)$ with the $\hat{E}_{cc}(4,2)$ diagrams.

Figure 3 gives the IED for $E^{(1)}_{\alpha\beta}$, $E^{(1)}_{\alpha\beta}$, and $E^{(3)}_{de}$ along with their symmetry factors. The remaining third-order IED can be found in Ref. 30 and is not reported here for the sake of brevity. We have 71 *ee* diagrams (1 is four body, 5 are five body, 27 are six body, 21 are seven body, and 17 are eight body) and 11 *cc* diagrams (1 four body, 5 five body, and 5 six body).

[1]M. H. Kalos, Phys. Rev. A **2**, 250 (1970); D. M. Ceperley and M. H. Kalos, in *Monte Carlo Method in Statistical Physics,* edited by K. Binder (Springer, Berlin, 1978).

[2]J. E. Hirsch, Phys. Rev. B **31**, 4403 (1985); J. E. Hirsch and H. Q. Lin, Phys. Rev. Lett. **31**, 4403 (1989).

[3]S. Sorella, E. Tosatti, S. Baroni, R. Car, and M. Parrinello, Int. J. Mod. Phys. B **1**, 993 (1988); S. Sorella, S. Baroni, R. Car, and M. Parrinello, Europhys. Lett. **8**, 663 (1989).

[4]A. Fabrocini and S. Fantoni, in *First International Course on Condensed Matter,* ACIF Series Vol. 8, edited by D. Prosperi, S. Rosati, and G. Violini (World Scientific, Singapore, 1986), and references therein.

[5]M. Viviani, A. Buendia, S. Fantoni, and S. Rosati, Phys. Rev. B **38**, 4523 (1988).

[6]S. Fantoni, B. Friedman, and V. R. Pandharipande, Nucl. Phys. **A386**, 1 (1982); **A339**, 1 (1983).

[7]J. R. Schrieffer, X. G. Wen, and S. C. Zhang, Phys. Rev. B **39**, 11 663 (1989).

[8]S. John, P. Voruganti, and W. Goff. Phys. Rev. B **43**, 13 365 (1991).

[9]C. Gros, R. Joynt, and T. M. Rice, Phys. Rev. B **36**, 381 (1987).

[10]H. Yokoyama and H. Shiba, J. Phys. Soc. Jpn. **56**, 1490 (1987); **56**, 3570 (1987); **56**, 3582 (1987).

[11]S. Fantoni, X. Q. Wang, E. Tosatti, and Lu Yu, Physica C **153**, 1255 (1988); S. Fantoni, X. Q. Wang, E. Tosatti, Lu Yu, and M. Viviani, Phys. Rev. B **41**, 11 479 (1991).

[12]J. Hubbard, Proc. R. Soc. London, Ser. A **276**, 238 (1964); **285**, 542 (1965).

[13]P. W. Anderson, Science **235**, 1196 (1987).

[14]W. F. Brinkman and T. M. Rice, Phys. Rev. B **2**, 4302 (1970).

[15]G. Shirane *et al.*, Phys. Rev.Lett. **59**, 1613 (1987). J. Tranquada *et al.*, *ibid.*, **60**, 156 (1988).

[16]K. B. Lyons *et al.*, Phys. Rev. B **37**, 2353 (1988); Phys. Rev. Lett. **60**, 732 (1988).

[17]E. H. Lieb and F. Y. Wu, Phys. Rev.Lett. **20**, 1445 (1968); F. H. L. Essler, V. E. Korepin, and K. Schoutens, *ibid.* **67**, 3848 (1991).

[18]W. Metzner and D. Vollhardt, Phys. Rev. Lett. **59**, 121 (1987); F. Gebhardt and D. Vollhardt, *ibid.* **59**, 1472 (1987).

[19]S. Fantoni and S. Rosati, Nuovo Cimento **20A**, 179 (1974); **25A**, 593 (1975).

[20]E. Krotscheck, Phys. Rev. A **15**, 397 (1977).

[21]M. Puoskari and A. Kallio, Phys. Scr. **24**, 601 (1981).

[22]G. Co', A. Fabrocini, S. Fantoni, and I. E. Lagaris (unpublished).

[23]F. Ristig, Z. Phys. B **79**, 351 (1990).

[24]S. Fantoni, Nuovo Cimento **44A**, 191 (1978).

[25]As it turns out, in the special case of the Gutzwiller operator, it is possible to use an *ad hoc* FHNC treatment, which explicitly makes use of the fact that $f(\mathbf{r}_{ij}\neq 0)=1$. This treatment is presented and discussed in a forthcoming paper. S. Fantoni, X. Q. G. Wang, E. Tosatti, and L. Yu (unpublished).

[26]The reduced diagrams in Table VI can be analytically calculated in the 1D case. The more complex diagrams are evaluated in terms of simpler ones, e.g., $L_8(\mathbf{r}_{12}) = [L_1(\mathbf{r}_{123})|L_6(\mathbf{r}_{32})]$, and $L_{12}(\mathbf{r}_{12})=L_2(\mathbf{r}_{12})L_3(\mathbf{r}_{12})$. In reduced diagrams, the simplest element connecting two points has only a factor $-1/\nu$ (Ref. 30).

[27]J. Carmelo, M. Dziermawa, X. Zotos, and D. Baeriswyl, Phys. Rev. B **43**, 598 (1991).

[28]The chemical potential jump $\bar{\Delta}$ at half-filling was calculated for the Lieb-Wu equations by S. Sorella (personal communication).

[29]X. Q. G. Wang, S. Fantoni, E. Tosatti, and L. Yu (unpublished).

[30]X. Q. G. Wang, Ph.D. thesis, SISSA, 1992.